# 3D NUMERICAL MODEL FOR PEARL RIVER ESTUARY

By K. W. Chau[1] and Y. W. Jiang[2]

**ABSTRACT:** A 3D numerical model with an orthogonal curvilinear coordinate in the horizontal direction and sigma coordinate in the vertical direction has been developed. This model is based on POM (Princeton Ocean Model). In this model a second moment turbulence closure submodel is embedded and the stratification caused by salinity and temperature is considered. Furthermore, to adapt to estuary locations where the flow pattern is complex, the horizontal time differencing is implicit with the use of a time-splitting method instead of the explicit method in POM. This model is applied to the Pearl River estuary, which is the largest river system in South China, with Hong Kong at the eastern side of its entrance. The computation is verified and calibrated with field measurement data. The computed results mimic the field data well.

## INTRODUCTION

The Pearl River (Zhujiang) is the largest river system in South China. The Pearl River Delta Region (PRDR), which includes eight cities (Guangzho, Shenzhen, Dongguan, Huizhou, Foshan, Zhongshan, and Jiangmen), is one of the most important economic zones in China, not to mention Asia and the world. With the economic boom of the PRDR, the resources of the estuary, such as the harbor, channel, and reclamation zone, have been exploited. Also, the water quality is deteriorating and red tides (algae blooms) have occurred several times in the past 2 years.

On July 1, 1997, the sovereignty and administration of Hong Kong were restored to the People's Republic of China. Since then more projects and concerns have focused on the area of the PRDR. Some models (2D or quasi-3D) have been developed to simulate the environmental hydraulics in the PRDR [e.g., Binnie and Partners (1988), Walker and Jones (1991), Chen and Li (1991), and Hu and Kot (1997)].

In this paper, a more complete 3D model is developed and the numerical model is based on POM (Princeton Ocean Model) (Mellor 1996). The principal attributes of the model that are described in this paper are as follows:

- It contains an embedded second moment turbulence closure submodel to provide vertical mixing coefficients.
- The curvilinear orthogonal coordinate is used in the horizontal direction, and the sigma coordinate is used in the vertical direction.
- The horizontal and vertical time differencing are treated semi-implicitly. A time-splitting method is used for the horizontal time differencing of the external mode.
- Complete thermodynamics have been implemented, and the stratification of salinity and temperature are considered.

The main difference between this model and POM is in the third attribute. In POM the horizontal time differencing is entirely explicit, but in this model the horizontal time differencing is semi-implicit with the use of a time-splitting method. The time step of this model is larger than that in POM. This attribute can be used in applications with complex flow patterns and large currents caused by the tide and river discharges, such as in the Pearl River estuary. A semi-implicit version of the Blumberg-Mellor model, ECOM-siz, has also been developed recently (Quamrul Ahsan and Blumberg 1999). In ECOM-siz, the barotropic pressure gradient in the momentum equations and horizontal velocity divergence in the continuity equation are treated implicitly and an untransformed vertical coordinate (*z*-level) system is used instead of the sigma coordinate system. The major differences with ECOM-siz are the time-splitting alternating direction implicit scheme in the external mode and sigma coordinate system employed.

The model is applied to the Pearl River estuary, which includes four outlets of the Pearl River system and the main part of Hong Kong seawaters (Fig. 1). This is probably the first application of this type of model (3D and baroclinic) in the PRDR. The model certainly has significance from an engineering point of view as a tool for exploring the dynamics and circulation of the PRDR. The computation is calibrated and verified with field measurement data.

## DESCRIPTION OF GOVERNING EQUATION AND SOLUTION METHOD

The model uses a sigma $\sigma$ coordinate condition in the vertical direction and an orthogonal curvilinear coordinate in the horizontal direction. In the $\sigma$ stretching system, $\sigma$ spans the range from $\sigma = 0$ at the surface of water to $\sigma = -1$ at the bottom. The $\sigma$ coordinate is more suitable for simulating current flow and salinity transportation than the *Z* system (Leedertse et al. 1973) because it provides the same number of layers regardless of water depth. This handles domains of large topographic variability well.

The curvilinear coordinate has become more popular in recent years because it can eliminate the stagger grid in a Cartesian coordinate system and improve the representation of the numerical model. There are two kinds of curvilinear coordinates, orthogonal and nonorthogonal. The orthogonal coordinate has the advantage that the motion equation is simpler, but it cannot generate a grid for a domain with complex geometry. Consequently, if the model is applied to a domain with a complex boundary, a nonorthogonal coordinate system is highly recommended.

The equations, which govern the dynamics of the coastal cycle, contain fast-moving external and slow-moving internal gravity waves. A splitting technique has been used (Simons 1974) to divide the 3D motion equations into two-part submodes, where one part is an internal mode (vertical structure) and the other part is an external mode (vertically averaged). The advantage of this technique is that it permits the calculation of free surface elevation with little sacrifice in computational time. This is achieved by solving the velocity transport separately from the 3D calculation of velocity and thermodynamic properties (Mellor 1996). The governing equations of the two submodes are written below.

[1]Assoc. Prof., Dept. of Civ. and Struct. Engrg., Hong Kong Polytechnic Univ., Hung Hom, Kowloon, Hong Kong.

[2]Res. Asst., Dept. of Civ. and Struct. Engrg., Hong Kong Polytechnic Univ., Hung Hom, Kowloon, Hong Kong.

Note. Discussion open until June 1, 2001. To extend the closing date one month, a written request must be filed with the ASCE Manager of Journals. The manuscript for this technical note was submitted for review and possible publication on March 15, 1999. This technical note is part of the ***Journal of Hydraulic Engineering***, Vol. 127, No. 1, January, 2001. ©ASCE, ISSN 0733-9429/01/0001-0072–0082/$8.00 + $.50 per page. Technical Note No. 20506.

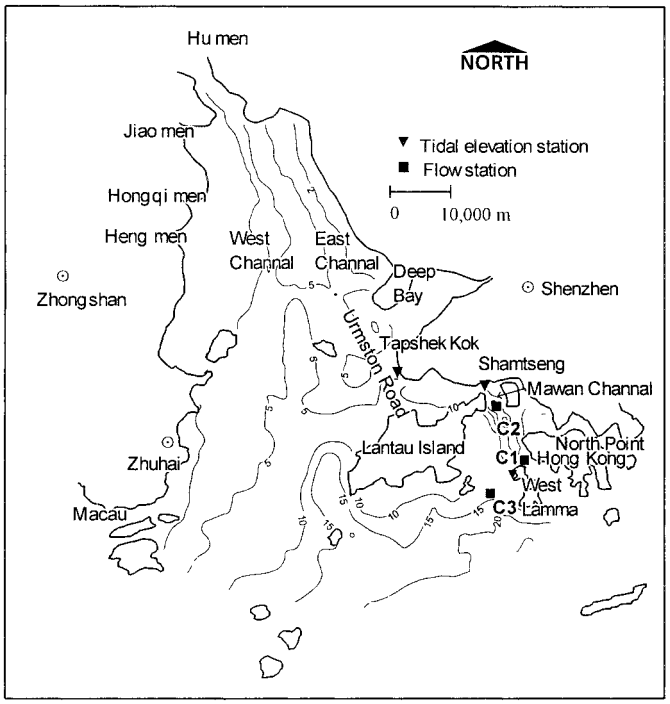


**FIG. 1. Topographic Map of Domain**

### Internal Mode

The internal model is a vertical structure mode described by the original 3D equations based on the σ coordinate system

Continuity equation:

$$\frac{\partial UD}{\partial x} + \frac{\partial VD}{\partial y} + \frac{\partial \omega}{\partial \sigma} + \frac{\partial \eta}{\partial t} = 0 \tag{1}$$

Momentum equation:

$$\frac{\partial UD}{\partial t} + \frac{\partial U^2 D}{\partial x} + \frac{\partial UVD}{\partial y} + \frac{\partial U\omega}{\partial \sigma} - fVD + gD\frac{\partial \eta}{\partial x} + \frac{gD^2}{\rho_0}\int_\sigma^0 \left[\frac{\partial \rho}{\partial x} - \frac{\sigma}{D}\frac{\partial D}{\partial x}\frac{\partial \rho}{\partial \sigma}\right] d\sigma = \frac{\partial}{\partial \sigma}\left[\frac{K_M}{D}\frac{\partial U}{\partial \sigma}\right] + F_x \tag{2}$$

$$\frac{\partial VD}{\partial t} + \frac{\partial UVD}{\partial x} + \frac{\partial V^2 D}{\partial y} + \frac{\partial V\omega}{\partial \sigma} + fUD + gD\frac{\partial \eta}{\partial y} + \frac{gD^2}{\rho_0}\int_\sigma^0 \left[\frac{\partial \rho}{\partial y} - \frac{\sigma}{D}\frac{\partial D}{\partial y}\frac{\partial \rho}{\partial \sigma}\right] d\sigma = \frac{\partial}{\partial \sigma}\left[\frac{K_M}{D}\frac{\partial V}{\partial \sigma}\right] + F_y \tag{3}$$

Temperature and salinity transport equation:

$$\frac{\partial TD}{\partial t} + \frac{\partial TUD}{\partial x} + \frac{\partial TVD}{\partial y} + \frac{\partial T\omega}{\partial \sigma} = \frac{\partial}{\partial \sigma}\left[\frac{K_H}{D}\frac{\partial T}{\partial \sigma}\right] + F_T \tag{4}$$

$$\frac{\partial SD}{\partial t} + \frac{\partial SUD}{\partial x} + \frac{\partial SVD}{\partial y} + \frac{\partial S\omega}{\partial \sigma} = \frac{\partial}{\partial \sigma}\left[\frac{K_H}{D}\frac{\partial S}{\partial \sigma}\right] + F_S \tag{5}$$

Turbulence energy equation:

$$\frac{\partial q^2 D}{\partial t} + \frac{\partial Uq^2 D}{\partial x} + \frac{\partial Vq^2 D}{\partial y} + \frac{\partial \omega q^2}{\partial \sigma} = \frac{\partial}{\partial \sigma}\left[\frac{K_q}{D}\frac{\partial q^2}{\partial \sigma}\right] + \frac{2K_M}{D}\left[\left(\frac{\partial U}{\partial \sigma}\right)^2 + \left(\frac{\partial V}{\partial \sigma}\right)^2\right] + \frac{2g}{\rho_0}K_H\frac{\partial \tilde{\rho}}{\partial \sigma} - \frac{2Dq^3}{B_1 l} + F_q \tag{6}$$

$$\frac{\partial q^2 lD}{\partial t} + \frac{\partial Uq^2 lD}{\partial x} + \frac{\partial Vq^2 lD}{\partial y} + \frac{\partial \omega q^2 l}{\partial \sigma} = \frac{\partial}{\partial \sigma}\left[\frac{K_q}{D}\frac{\partial q^2 l}{\partial \sigma}\right] + E_1 l\frac{K_M}{D}\left[\left(\frac{\partial U}{\partial \sigma}\right)^2 + \left(\frac{\partial V}{\partial \sigma}\right)^2\right] + E_1 E_3 l\frac{g}{\rho_0}K_H\frac{\partial \tilde{\rho}}{\partial \sigma} - \tilde{W}\frac{Dq^3}{B_1} + F_l \tag{7}$$

The horizontal viscosity and diffusion terms are defined according to

$$F_x = \frac{\partial}{\partial x}(H\tau_{xx}) + \frac{\partial}{\partial y}(H\tau_{xy}) \tag{8}$$

$$F_y = \frac{\partial}{\partial x}(H\tau_{xy}) + \frac{\partial}{\partial y}(H\tau_{yy}) \tag{9}$$

$$F_\phi = \frac{\partial}{\partial x}(Hq_x) + \frac{\partial}{\partial y}(Hq_y) \tag{10}$$

where

$$\tau_{xx} = 2A_M\frac{\partial U}{\partial x};\quad \tau_{xy} = \tau_{yx} = A_M\left[\frac{\partial U}{\partial y} + \frac{\partial V}{\partial x}\right]$$

$$\tau_{yy} = 2A_M\frac{\partial V}{\partial y};\quad q_x = A_H\frac{\partial \phi}{\partial x};\quad q_y = A_H\frac{\partial \phi}{\partial y}$$

where $\phi$ represents $T$, $S$, $q^2$, and $q^2 l$. In the above equations, $U$, $V$, and $\omega$ = mean fluid velocities in the $x$-, $y$-, and σ-direc-

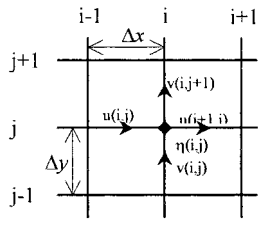


**FIG. 2. Arakawa C Grids**

**TABLE 1. Discharge of Four Eastern Outlets in Different Seasons**

| Year (1) | Hu Men Wet (2) | Hu Men Mean (3) | Hu Men Dry (4) | Jiao Men Wet (5) | Jiao Men Mean (6) | Jiao Men Dry (7) | Hongqi Men Wet (8) | Hongqi Men Mean (9) | Hongqi Men Dry (10) | Heng Men Wet (11) | Heng Men Mean (12) | Heng Men Dry (13) |
|---|---|---|---|---|---|---|---|---|---|---|---|---|
| 1985 | 303.5 | 158.7 | 108.1 | 290.2 | 146.4 | 93.5 | 112.6 | 51.6 | 27.6 | 190.4 | 90.6 | 59.8 |
| 1986 | 341.4 | 126.2 | 58.9 | 326.4 | 116.4 | 50.9 | 126.7 | 41.0 | 15.0 | 214.2 | 72.1 | 32.6 |
| 1987 | 284.4 | 149.3 | 66.2 | 271.9 | 137.8 | 57.3 | 105.5 | 48.5 | 16.9 | 178.4 | 85.3 | 36.6 |
| 1988 | 294.5 | 123.6 | 72.4 | 281.6 | 114.0 | 62.6 | 109.3 | 40.2 | 18.4 | 184.8 | 70.6 | 40.0 |
| 1989 | 219.1 | 97.4 | 68.0 | 209.5 | 89.8 | 58.7 | 81.3 | 31.7 | 17.3 | 137.5 | 55.6 | 37.6 |
| 1990 | 260.9 | 187.5 | 96.2 | 249.5 | 172.9 | 83.2 | 96.8 | 60.9 | 24.5 | 163.7 | 107.1 | 53.2 |
| 1991 | 242.6 | 79.3 | 63.6 | 232.0 | 73.2 | 55.0 | 90.0 | 25.8 | 16.2 | 152.2 | 45.3 | 35.2 |
| 1992 | 289.7 | 133.2 | 109.0 | 277.0 | 122.9 | 94.2 | 107.5 | 43.3 | 27.8 | 181.8 | 76.1 | 60.3 |
| 1993 | 397.2 | 131.9 | 61.5 | 379.8 | 121.7 | 53.2 | 147.4 | 42.9 | 15.7 | 249.2 | 75.3 | 34.0 |
| 1994 | 500.9 | 171.5 | 84.4 | 478.9 | 158.2 | 73.0 | 185.8 | 55.7 | 21.5 | 314.2 | 97.9 | 46.7 |
| 1995 | 307.8 | 188.1 | 104.9 | 294.3 | 173.5 | 90.7 | 114.2 | 61.1 | 26.8 | 193.1 | 107.4 | 58.0 |
| Average | 312.9 | 140.6 | 81.2 | 299.2 | 129.7 | 70.2 | 116.1 | 45.7 | 20.7 | 196.3 | 80.3 | 44.9 |

Note: Wet season months: May–September; mean season months: April, October, and November; dry season months: December–March. Unit: $10^8$ $m^3$/season.

tions, respectively; $\eta$ = elevation of sea surface above the undisturbed level; $f$ = Coriolis parameter; $D = \eta + H$, where $H$ = depth of the water and $g$ = Earth's gravitational acceleration; $\rho_0$ = fluid density; $\rho$ = fluid density after subtraction of the horizontally averaged density; $\tilde{\rho}$ = buoyant fluid density; $T$ = temperature; $S$ = salinity; $q^2$ = turbulence energy; $l$ = mixing length; $K_M$, $K_H$, and $K_q$ = vertical turbulent flux coefficients; $A_M$ and $A_H$ = horizontal turbulent coefficients; $\tilde{W}$ = wall proximity function; and $B_1$, $E_1$, and $E_3$ = constants determined from laboratory experiments.

From these equations, it can be seen that a $q^2$-$q^2l$ turbulence model is considered. It involves two prognostic equations, in essence, identical to those used in the $K$-$\varepsilon$ approach (Davies et al. 1997).

## External Mode

The external mode, which is integrated vertically by the continuity and momentum equations, can be written as 2D dynamic equations

Continuity equation:

$$\frac{\partial \bar{U}D}{\partial x} + \frac{\partial \bar{V}D}{\partial y} + \frac{\partial \eta}{\partial t} = 0 \tag{11}$$

Momentum equation:

$$\frac{\partial \bar{U}D}{\partial x} + \frac{\partial \bar{U}^2 D}{\partial x} + \frac{\partial \bar{U}\bar{V}D}{\partial y} - \tilde{F}_x - f\bar{V}D + gD\frac{\partial \eta}{\partial x} = \langle wu(-1)\rangle - \frac{gD}{\rho_0}\int_{-1}^{0}\int_{\sigma}^{0}\left[D\frac{\partial \rho}{\partial x} - \frac{\sigma \partial D}{\partial x}\frac{\partial \rho}{\partial \sigma}\right]d\sigma\, d\sigma \tag{12}$$

$$\frac{\partial \bar{V}D}{\partial t} + \frac{\partial \bar{U}\bar{V}D}{\partial x} + \frac{\partial \bar{V}^2 D}{\partial y} - \tilde{F}_y + f\bar{U}D + gD\frac{\partial \eta}{\partial y} = \langle wv(-1)\rangle - \frac{gD}{\rho_0}\int_{-1}^{0}\int_{\sigma}^{0}\left[D\frac{\partial \rho}{\partial y} - \frac{\sigma \partial D}{\partial y}\frac{\partial \rho}{\partial \sigma}\right]d\sigma\, d\sigma \tag{13}$$

where $(\underline{wu}(-1), \underline{wv}(-1)) = -C_Z(U^2 + V^2)^{1/2}(\underline{U}, \underline{V})$, $\sigma \to -1$; $\bar{U}$ and $\bar{V}$ = vertically integrated velocities; $(\bar{U}, \bar{V}) = \int_{-1}^{0}(U, V)\, d\sigma$; $\tilde{F}_x$ and $\tilde{F}_y$ = horizontal turbulence diffusion terms; $\langle wu(-1)\rangle$ and $\langle wv(-1)\rangle$ = bottom stress components; and $C_Z$ = Chézy coefficient.

## Interaction of Internal and External Modes

The velocity advection [the second and third terms of (12) and (13)], horizontal diffusion (the fourth term) and density gradient (the eighth term) are integrated vertically from the corresponding terms of the internal equations. In (12) and (13), the bottom stress is derived from the velocity of the internal mode. On the other hand, when computing the internal mode, the elevation of the water surface is obtained directly from the external mode. The internal and external modes have different truncation errors, so the vertical integrals of the internal mode velocity may differ slightly from $\bar{U}$ and $\bar{V}$. To eliminate the current velocity of the internal mode $(U, V)$ is adjusted to fit the following condition:

$$\int_{-1}^{0} U\, d\sigma = \bar{U}$$

## Structure of Internal Mode Calculation

For a detailed description of the internal mode, refer to Blumberg and Mellor (1980, 1987) and Mellor (1996). The method is semi-implicit and all terms of (2) and (3) are treated explicitly except for the vertical flux (the first term on the right-hand side), which is treated implicitly. All equations here are based on Cartesian coordinates; readers can refer to Chau and Jin (1995) for equations under the orthogonal curvilinear coordinates.

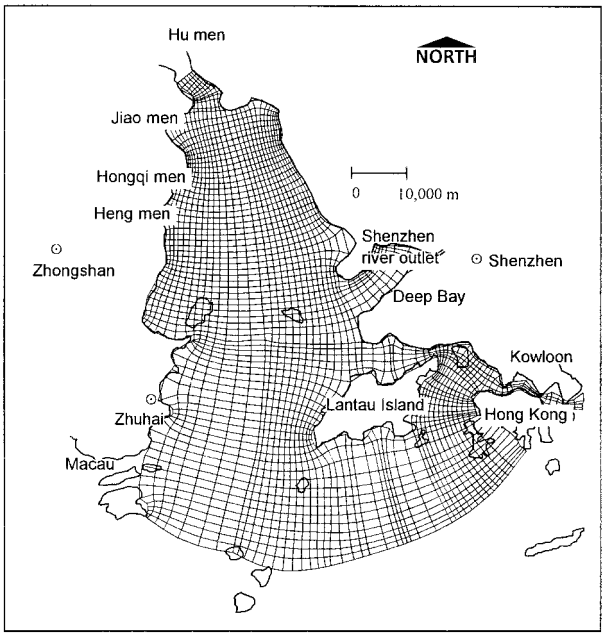


**FIG. 3. Orthogonal Curvilinear Grid**

## Structure of External Mode Calculation

The solution of the external mode in POM is entirely explicit and uses the C-grid. The time step is based on the Courant-Friendrichs-Lewy condition, which requires the condition

$$dt < \frac{dx}{\sqrt{2gh}} + U_{\max}/\sqrt{2}$$

For small grid sizes, the corresponding time step will be set small to keep the computation stable, which will then require a large amount of time.

To develop a 3D numerical model that can represent the Pearl River estuary (the smallest size of the generated orthogonal curvilinear grid is 50 m) and operate on a personal computer with Pentium II, a semi-implicit method is used in the external mode. This method is expressed as a time-splitting alternating direction implicit scheme on the ''Arakawa C'' grids, as shown in Fig. 2 (Chau and Jin 1995).

*x*-direction continuity equation:

$$\frac{\eta^*_{i,j} - \eta^n_{i,j}}{\Delta t} + \frac{\bar{U}^*_{i+1,j}(D^n_{i,j} + D^n_{i+1,j}) - \bar{U}^*_{i,j}(D^n_{i-1,j} + D^n_{i,j})}{2\Delta x} + \frac{\bar{V}^n_{i,j+1}(D^n_{i,j} + D^n_{i,j+1}) - \bar{V}^n_{i,j}(D^n_{i,j-1} + D^n_{i,j})}{2\Delta v} = 0 \quad (14)$$

*x*-direction momentum equation:

$$\frac{\bar{U}^*_{i,j} - \bar{U}^n_{i,j}}{\Delta t} + g\frac{\eta^*_{i+1,j} - \eta^*_{i,j}}{\Delta x} - f\frac{\bar{V}^n_{i-1,j} + \bar{V}^n_{i-1,j+1} + V^n_{i,j} + \bar{V}^n_{i,j+1}}{4} = A^n \quad (15)$$

*y*-direction continuity equation:

$$\frac{\eta^{n+1}_{i,j} - \eta^*_{i,j}}{\Delta t} + \frac{\bar{V}^{n+1}_{i,j+1}(D^*_{i,j} + D^*_{i,j+1}) - \bar{V}^{n+1}_{i,j}(D^n_{i,j} + D^n_{i,j+1})}{2\Delta y} - \frac{\bar{V}^n_{i,j+1}(D^n_{i,j} + D^n_{i,j+1}) - V^n_{i,j}(D^n_{i,j-1} + D^n_{i,j})}{2\Delta y} = 0 \quad (16)$$

*y*-direction momentum equation:

$$\frac{\bar{V}^{n+1}_{i,j} - \bar{V}^n_{i,j}}{\Delta t} + g\frac{\eta^{n+1}_{i,j+1} - \eta^{n+1}_{i,j}}{\Delta y} + f\frac{\bar{U}^*_{i-1,j} + \bar{U}^*_{i-1,j+1} + \bar{U}^*_{i,j} + \bar{U}^*_{i,j+1}}{4} = B^n \quad (17)$$

At the end of each time step the following equation is assured:

$$\bar{U}^{n+1}_{i,j} = \bar{U}^*_{i,j} \quad (18)$$

where $\eta^*$ and $\bar{U}^*$ = two middle unknowns in the first time-splitting step in the *x*-direction; and $A^n$ and $B^n$ = terms that can be obtained from the internal submode. Equations in each direction can be written in a tridiagonal matrix and solved with the use of the double-sweep algorithm method (Leedertse and Crittion 1971). The solution consists of two time-splitting steps that advance the solution, first, from time level *nt* to *t** in the *x*-direction, which gives $\bar{U}^*$ and $\eta^*$, and second, from *t** to $(n + 1)t$ in the *y*-direction, which is how $\bar{V}^{n+1}$ and $\eta^{n+1}$ are obtained. Finally let $\bar{U}^{n+1} = \bar{U}^*$.

## Numerical Stability

Because the numerical scheme used here is semi-implicit, the terms of vertical diffusion in the internal mode and the elevation gradation term in the external mode are treated implicitly. The time step of numerical computation cannot exceed the limits associated with the advection, Coriolis, baroclinic pressure gradient, and horizontal diffusion terms. The semi-implicit numerical algorithm permits a time step many times greater than that based upon the Courant-Friendrichs-Lewy condition. From the computational experiments of this model applied in the Pearl River estuary, the maximum time step of the external mode is 100 s and the maximum time step of the internal mode is 60 s. Simply, this model uses the same time step, 60 s, in both submodes. If POM is applied in the research area with the same grid, the maximum time steps are 6 s and 100 s for external and internal modes, respectively. The model described here requires a core memory of 14.8 megawords and about 20 s/h run time. On the other hand, POM needs 14.2 megawords memory and 28 s/h run time based on a PII-450 PC.

## Errors Caused by Sigma Coordinate Pressure Gradient

Numerical models using sigma coordinates have the capability of dealing with an ocean application with a large topographic variability. The disadvantage of this model, however, is its hydrostatic inconsistency due to the bottom topography

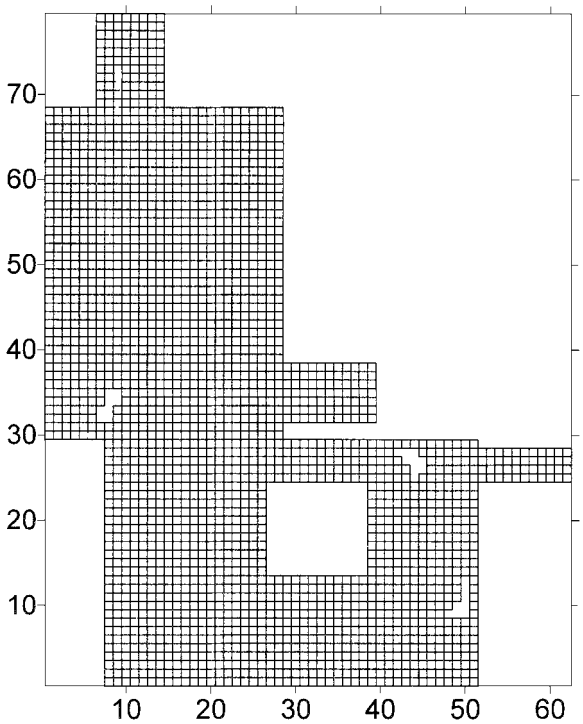


**FIG. 4. Transformed Plane**

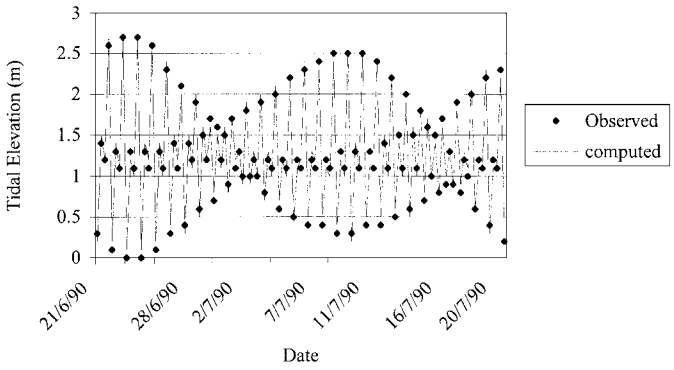


**FIG. 5. Comparison of Tidal Elevation Results versus Observations at West Lamma from June 21 to July 20, 1990**

effect. This inconsistency is caused by the horizontal density gradient along the constant σ layer. Mellor et al. (1997) utilized some strategies, which have been used in this model, to reduce these inconsistencies. The first is to examine the topography and adjust $H$ (depth of water) so that $H$ can fit the equation given by Haney (1990)

$$\left|\frac{\sigma}{H}\frac{\partial H}{\partial x}\right| \delta x < \delta\sigma$$

The second method adopted in this model is to subtract a climatological density (or temperature and salinity) before computing fluxes. The climatological density (or temperature and salinity) fields can be set to

$$d\rho_{c\,\mathrm{lim}}/dt = a(\rho - \rho_{c\,\mathrm{lim}}) \tag{19}$$

where $a$ = inverse of decay time; and $\rho$ and $\rho_{c\,\mathrm{lim}}$ = density and climatological density, respectively. The value of $a$ adopted in this Pearl River estuary model is $(1/t)$, where $t$ is the period of major tidal constituent. In this model $t = 0.5175$ day, which is the period of M2 (Ip and Wai 1990).

## Application of Model to Pearl River Estuary

The Pearl River estuary has been established as a very important zone in South China. With the economy quickly developing in this area, the environment has been deteriorating; hence, more and more attention is being put on research in this estuary. Because the hydrodynamic numerical model is an efficient tool for an environmental impact assessment and feasibility study of projects, the model has been applied to this estuary and calibrated.

The study area (Fig. 1) is a delta estuary. The depth of the open side of the estuary ranges from 20 to 28 m and becomes shallower toward the inner bay. The mean depth of the estuary is 7 m. There are four river outlets in the northwest of the estuary (Hu men, Jiao men, Heng men, and Hongqi men). Based on the published data (Pang and Li 1998), the net dis-

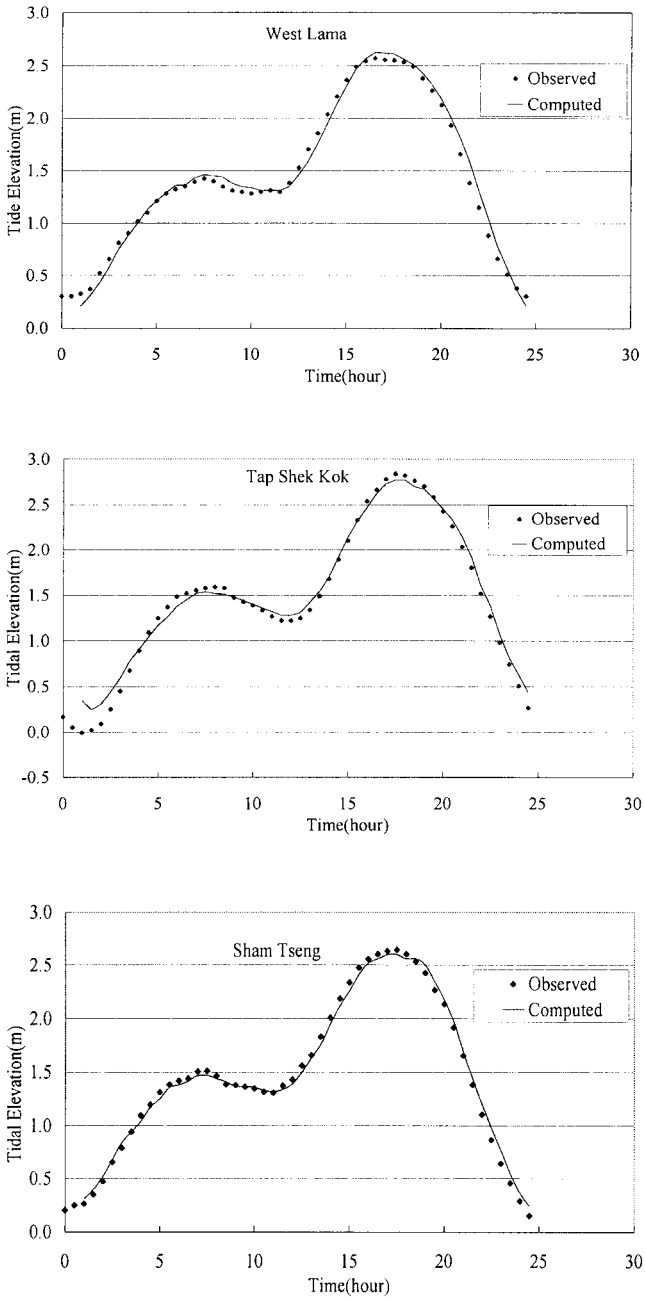


**FIG. 6. Calibration of Tidal Elevation from June 21 to 22, 1990 at: (a) West Lamma; (b) Tap Shek Kok; (c) Sham Tseng**

charges for the four outlets in different seasons are listed in Table 1. It can be seen that the discharges in different years vary greatly. The tide in the Pearl River estuary is semidiurnal and irregular. The mean tidal range is about 1.0 m. At the entrance of the estuary, the mean tidal range is 0.85–0.95 m. The range is higher in the inner estuary. The mean tidal range in Hu men is 1.6 m (Kot and Hu 1995). In the wet season (May–September) the runoff to the rivers is strongest and becomes the predominant hydrodynamic force in the Pearl River estuary, whereas in the dry season (December–March) the tidal current is the main force (Lu 1997).

The horizontal grid of the orthogonal curvilinear coordinate system is displayed in Fig. 3, and the corresponding transformed grid is shown in Fig. 4. There are 3,400 grids in each of the six vertical layers. Each layer has the same $\delta\sigma = 1/6$. The number of layer and grid points are chosen such that reasonable accuracy is achieved in horizontal and vertical discretizations while computational efficiency is not deterred.

## Open Boundary Condition

At the open boundaries (southern and eastern boundaries), the tide elevation is the model force. It can be interpolated from the observed data at two stations (Macau and North Point) according to tidal wave propagating speed $\sqrt{gh}$ (Huang and Lu 1995). The velocity values of external and internal modes at the open boundary are derived from the radiation condition; for example, at the southern open boundary

$$\frac{\partial v}{\partial t} - c_i \frac{\partial v}{\partial y} = 0, \quad c_i = \sqrt{H/H_{\max}}$$

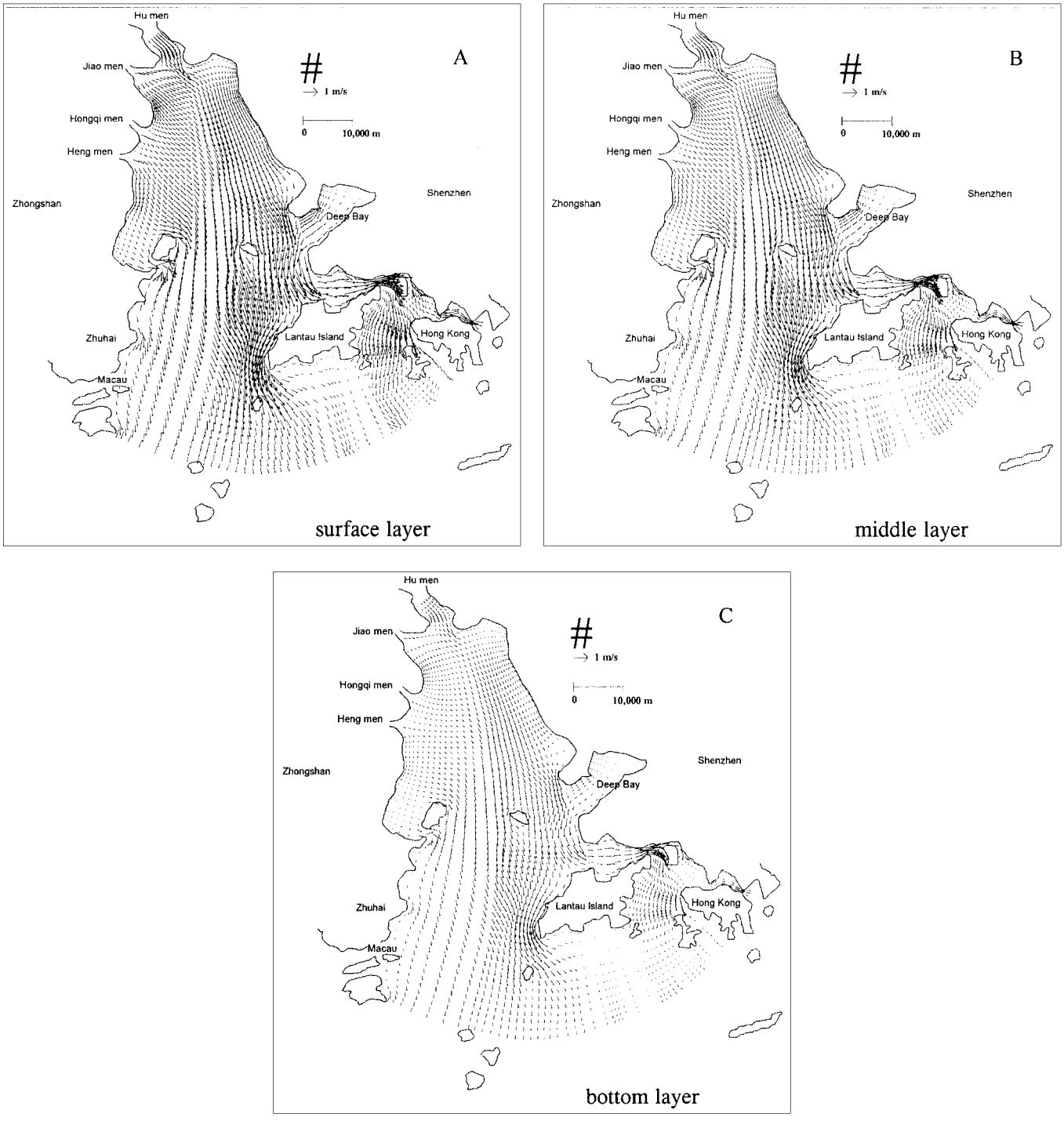


**FIG. 7. Ebb Tidal Flow Field in Three Layers in Mean Season: (a) Surface; (b) Middle; (c) Bottom**

The values of salinity, temperature, turbulence kinetic, and turbulence dissipation at the open boundary condition are derived from the following equations:

Ebb time:

$$\frac{\partial A}{\partial t} + U\frac{\partial A}{\partial x} = 0 \tag{20}$$

Flood time:

$$A = A_{set}(t, \sigma) \tag{21}$$

where $A$ represents the salinity, temperature, turbulence kinetic, and turbulence dissipation. During ebb, at open boundaries, $A$ is calculated using the ''upwind'' differenced advective equation. During flood, $A$ is linearly interpolated from its value at the end of ebb to a fixed $A$ that depends on the depth and observed data. The open boundary conditions of the four outlets in the northwest of the research area are governed by water discharges.

## Closed Boundary Conditions

The convection and diffusion terms require the value of the velocity at the outer boundary to close the motion equations. Two kinds of closed boundary conditions have been tested in this model. For $\partial u/\partial y$, the first is a no-slip condition that assumes $u = 0$ and the second is a free-slip condition in which $\partial u/\partial y = 0$. The model applied to the Pearl River estuary weighs the two methods together and gets the semislip boundary condition

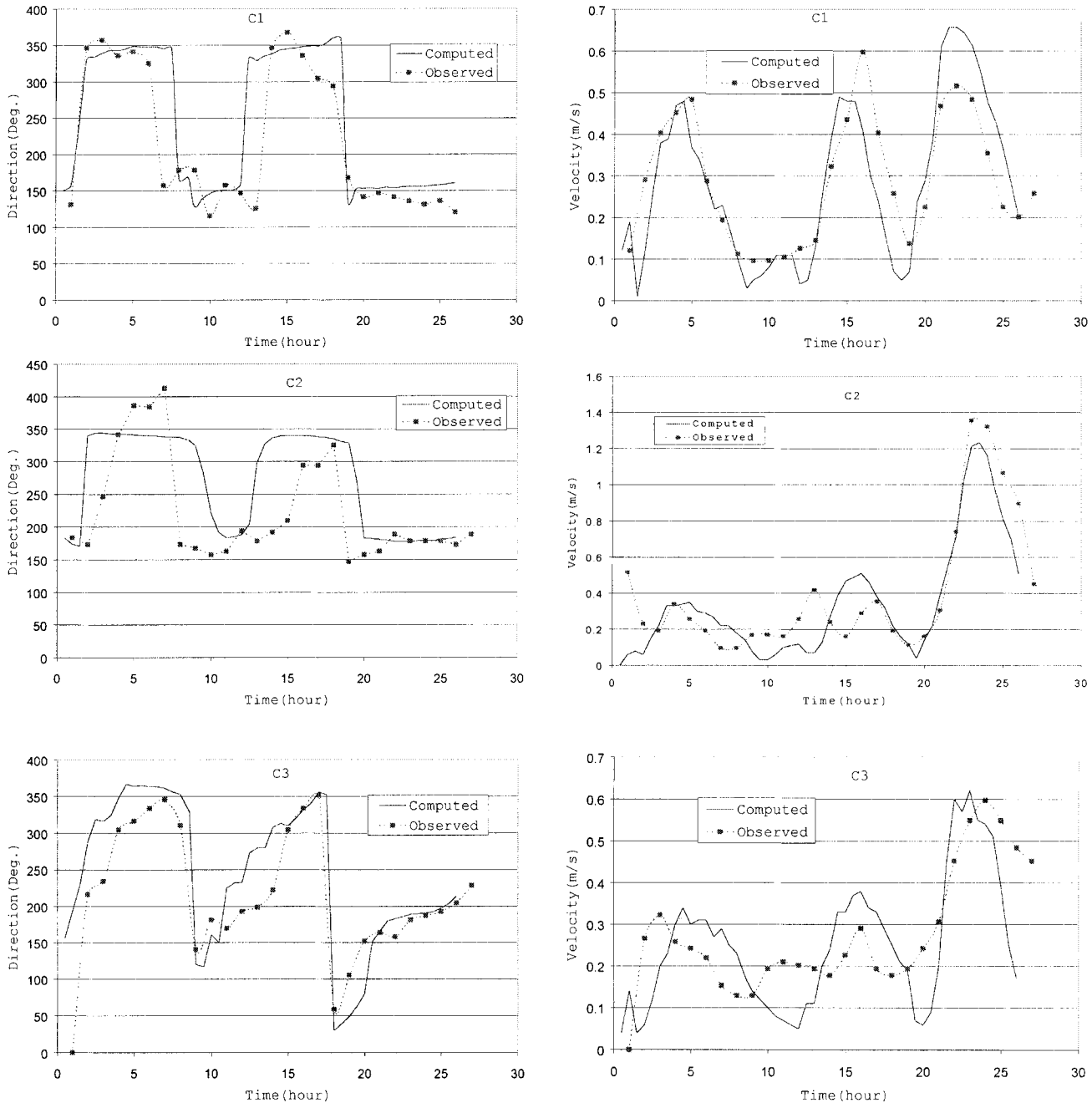


**FIG. 8. Calibration of Tidal Flow Direction and Velocity from June 21 to 22, 1990 in Three Stations (C1, C2, and C3)**

$$\frac{\partial u}{\partial y} = \frac{\beta u}{\Delta y}, \quad 0 \leq \beta \leq 1$$

Sensitivity tests with different $\beta$ values have been conducted, with little change in the results.

## CALIBRATIONS

In June–July 1990, the Hong Kong Civil Engineering Department, Port Development Division, carried out a hydrological survey. The survey data observed at three tidal elevation stations and three tidal current stations were used for calibration of this model. Fig. 1 shows the location of these stations. The observed data from June 21 to July 20, 1990, of tidal elevation at two stations, Macau and Northpoint, are available to be used as boundary conditions. The model simulated 1 month's hydrodynamics of the Pearl River estuary in this period.

To calibrate the simulations, the computational results of three components have been verified with the corresponding observed data. The three components are tidal elevation, flow velocity, and direction. Because of the lack of detailed salinity data, only the salinity contour is shown.

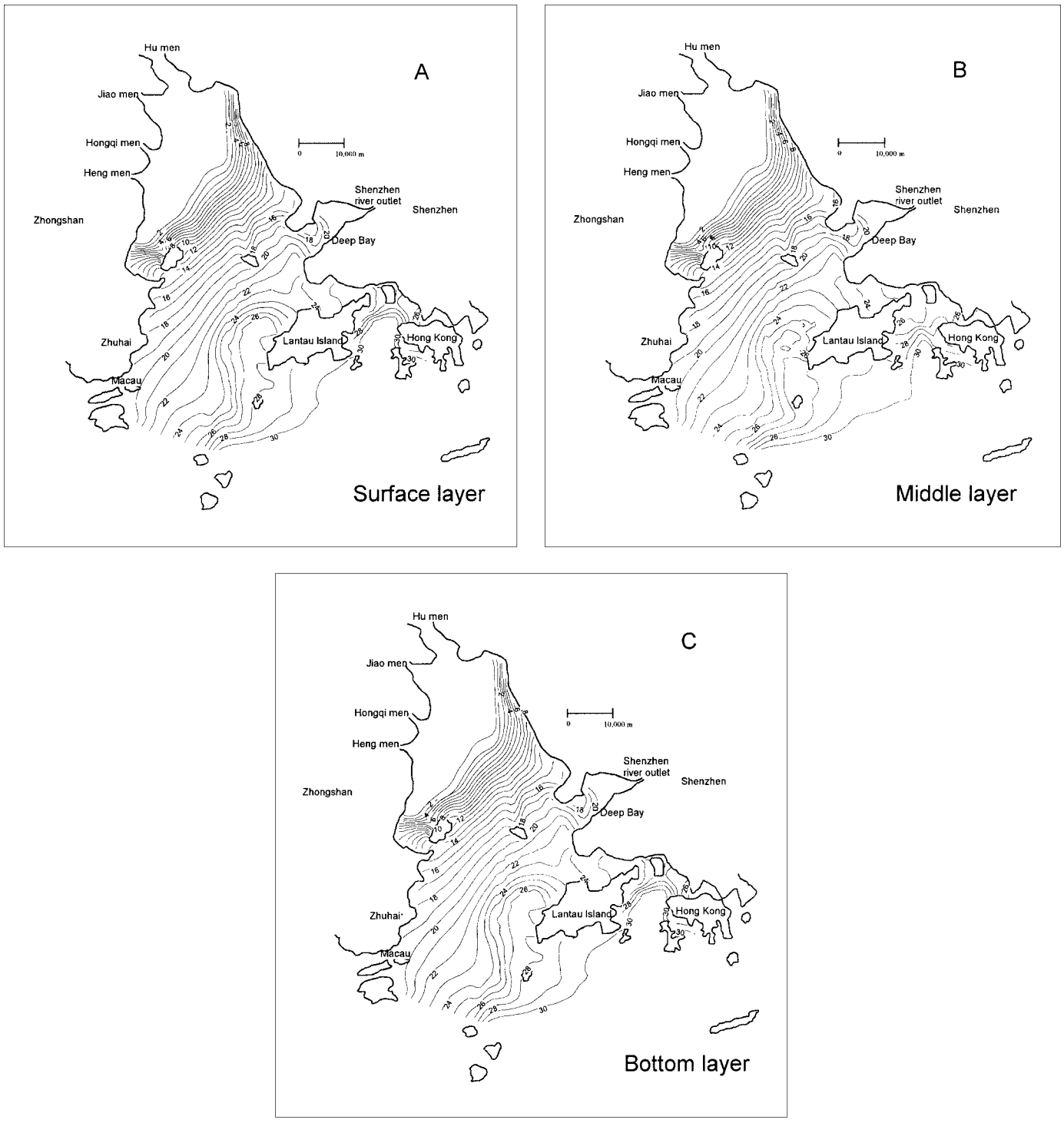


**FIG. 9. Computed Salinity Contour of Three Layers in Wet Season: (a) Surface; (b) Middle; (c) Bottom**

### Calibration of Tidal Elevation

The entire month's comparison of elevation results versus observations (from June 21 to July 20, 1990) at West Lamma is shown in Fig. 5. However, a typical 25 h of comparison can more effectively illustrate the slight differences between the computed results and observations. Fig. 6 illustrates the computational and measured results of tidal elevation at three different elevation stations from 15:30 on June 21 to June 22, 1990. It appears that the computational results concur well with the measured data. From this figure it is clear that the amplitude of the inner stations (such as Tap Shek Kok) is larger than the outer stations (such as West Lamma).

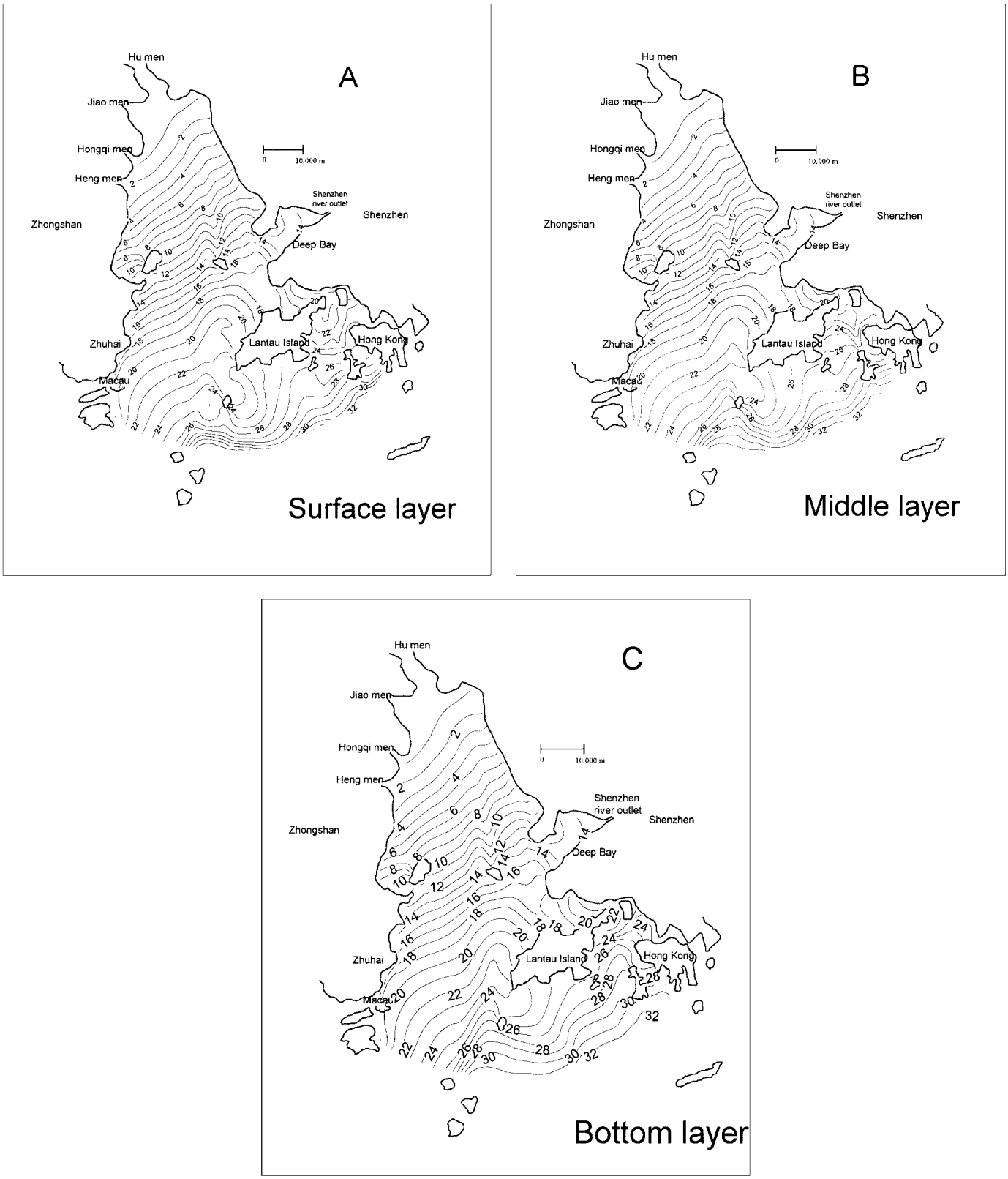


**FIG. 10. Computed Salinity Contour of Three Layers In Dry Season: (a) Surface; (b) Middle; (c) Bottom**

### Calibration of Tidal Flow

Fig. 7 shows the horizontal tidal current pattern during an ebb tide in the mean season (April, October, and November) at the surface, middle, and bottom layers, respectively, in the Pearl River estuary.

In this figure, the current velocities at the surface are slightly faster than at the bottom. The flow directions at the surface and bottom layers may be slightly nonuniform, especially when the current is not too fast. The maximum flow velocity (2.5 m/s) occurs at narrow channels in Ma Wan Channel and Kap Shui Mun where the water depth is >20 m. The current speed in the northwest Lantau Island water areas, Urmston Road and West East Channel, are higher than other locations because the bathymetry of these locations causes lateral contraction in the flow channel; hence, faster flows are also expected there. In general, the simulated current pattern agrees well with the observed data (Kot and Hu 1995).

The depth-averaged velocities at the three tidal stations are compared with the observed data. Fig. 8 shows the results of a comparison of direction and magnitude of velocity between computed and observed data from 15:30 on June 21 to June 22, 1990. The root-mean-square errors of the computed tidal level, flow direction, and velocity for the 1-month comparisons are 0.14 m, 17°, and 0.07 m/s, respectively. The computed flow direction and velocity coincide well with the observed data, which indicates that the model can simulate the observed data well.

As can be seen in Figs. 6 and 8, start-up of the simulation requires about 2–3 h before it converges to the accurate solution and matches with the observations well.

### Distribution of Salinity

The distribution of salinity in the wet and dry seasons is simulated. The measured data, such as tidal level and salinity at the open boundary from June 21 to July 20, 1990, are used as the boundary conditions in the wet season. Due to lack of data in winter, the same tidal levels are used to simulate the salinity distribution in the dry season. The salinity at the open boundary is derived from the dry season salinity horizontal and vertical patterns given by Kot and Hu (1995) and Broom and Ng (1995). The discharges of the four rivers are used as the data for the wet and dry seasons in 1990 (Table 1).

As seen from the distribution of salinity during ebb tide in three layers (Fig. 9), a sharp change of salinity is a common phenomenon in the Pearl River estuary during the wet season. This figure indicates that the stratification is only discernible in the outer bay and breaks down in the inner bay because the water depth becomes shallower and turbulence becomes stronger. In the dry season (Fig. 10), the sharp gradient of salinity or stratification is not so notable and the seawater intrusion is farther into the inner delta area. Therefore, in the inner delta, the gradient of salinity is smaller but the average salinity is higher than in summer. The pattern of the distribution of salinity shows no discrepancy with the pattern described by Kot and Hu (1995).

## CONCLUSIONS

A 3D curvilinear hydrodynamic model has been formulated, verified, and applied to the Pearl River estuary. This region is the most quickly developing in China, with Hong Kong and Macau at its entrance.

In this model, the external and internal gravity waves have been split in the analysis. The former becomes a 2D mode (external mode), and the latter forms a 3D mode (internal mode). In the external mode, the term of tidal elevation gradient is treated implicitly and the other terms are integrated or obtained from the internal mode. In the internal mode, the vertical flux term of the momentum equation is treated implicitly and tidal elevation values come directly from the external mode. The same time step is adopted in internal and external modes. With the use of these methods, the time step is larger than POM; hence, less computational time is needed to keep the computation stable.

The model is applied to the Pearl River estuary with the stratification, caused by the salinity and temperature, considered. The computational results of tidal elevation, direction, and magnitude of the current velocity are compared with the measured data in July 1990. The result shows fairly good agreement between the simulated and survey-measured data. The distribution of salinity in different layers during the west and dry seasons has been illustrated.

Above all, a complicated and efficient 3D model has been developed. It works well when applied to the Pearl River estuary, which is a typical estuary domain.

## ACKNOWLEDGMENT

The work described in this paper was substantially supported by a grant from the Research Grants Council of the Hong Kong Special Administrative Region (Project No. PolyU 5084/97E).

## APPENDIX. REFERENCES

Binnie and Partners. (1988). *Hydraulic and water quality studies in Victoria Harbor*, Territory Devel. Dept., Hong Kong Government, Hong Kong.

Blumberg, A. F., and Mellor, G. L. (1980). ''A coastal ocean numerical model.'' *Proc., Int. Symp., Math Modelling of Estuarine Phys.*, J. Sunderman and K.-P. Holtz, eds., Springer, Berlin, 203–214.

Blumberg, A. F., and Mellor, G. L. (1987). ''A description of a three-dimensional coastal ocean circulation model.'' *Three-dimension coastal ocean models*, Vol. 4, N. Heaps, ed., American Geophysical Union, Washington, D.C., 208.

Broom, M. J., and Ng, A. K. M. (1995). *Water quality Hong Kong and the influence of the Pearl River, Coastal infrastructure development in Hong Kong—A review*, Hong Kong Government, Hong Kong.

Chau, K. W., and Jin, H. S. (1995). ''Numerical solution of two-layered, two-dimensional tidal flow in boundary-fitted orthogonal curvilinear coordinate system.'' *Int. J. Numer. Methods in Fluids*, 21(11), 1087–1107.

Chen, H. Y., and Li, Y. S. (1991). ''A three-dimensional semi-implicit finite-difference model for flows in stratified seas.'' *Environmental hydraulics*, J. Lee and Y. K. Cheng, eds., Balkema, Rotterdam, The Netherlands, 937–942.

Davies, A. M., Jones, J. E., and Xing, J. (1997). ''Review of recent developments in tidal hydrodynamic modeling. II: Turbulence energy models.'' *J. Hydr. Engrg.*, ASCE, 123(4), 293–302.

Haney, R. L. (1990). ''Notes and Correspondence: On the pressure gradient force over steep topography in sigma coordinate ocean model.'' *J. Phys., Oceanography*, 21(4), 610–619.

Hu, S. L., and Kot, S. C. (1997). ''Numerical model of tides in Pearl River estuary with moving boundary.'' *J. Hydr. Engrg.*, ASCE, 123(1), 21–29.

Huang, S., and Lu, Q. M. (1995). *Estuarine dynamics*, Water Conservancy and Electricity Press, Beijing, 11–20.

Ip, S. F., and Wai, H. G. (1990). ''An application of harmonic method to tidal analysis and prediction in Hong Kong.'' *Hong Kong Tech. Note (local) No. 55*, Royal Observatory, Hong Kong.

Kot, S. C., and Hu, S. L. (1995). ''Water flows and sediment transport in Pearl River estuary and wave in South China sea near Hong Kong.'' *Coastal infrastructure development in Hong Kong—A review*, Hong Kong Government, Hong Kong, 13–32.

Leedertse, J. J., Alexander, R. C., and Liu, S. K. (1973). ''A three-dimensional model for estuaries and coastal seas, Volume I. Principles of computation.'' *R-1417-OWRR*, Rand Corp., Santa Monica, Calif.

Leedertse, J. J., and Crittion, E. C. (1971). ''A water quality simulation model for well mixed estuaries and coastal seas. Computation procedures.'' *R-708-NYC*, Rand Corp., New York.

Lu, Q. M. (1997). ''Three-dimensional modeling of hydrodynamics and sediment transport with parallel algorithm.'' PhD thesis, Hong Kong Polytechnic University, Hong Kong.

Mellor, G. L. (1996). *User's guide for a three-dimensional, Primitive equation, numerical ocean model*, Princeton University, Princeton, N.J.
Mellor, G. L., Oey, L. Y., and Ezer, T. (1997). ''Sigma coordinate pressure gradient errors and the seamount problem.'' *J. Atmospheric and Ocean Technol.*, 15(5), 1122–1131.
Pang, Y., and Li, X. L. (1998). ''Study of pollutants passing through the four east outlets of Pearl River Delta to Lingding sea.'' *Proc., Workshop on Hydr. of the Pearl River Estuary*, Y. S. Li, ed., 85–98.
Quamrul Ahsan, A. K. M., and Blumberg, A. F. (1999). ''Three-dimensional hydrothermal model of Onondaga Lake, New York.'' *J. Hydr. Engrg.*, ASCE, 125(9), 912–923.
Simons, T. J. (1974). ''Verification of numerical models of Lake Ontario. Part 1, circulation in spring and early summer.'' *J. Phys., Oceanography*, 4(4), 507–523.
Walker, A. F., and Jones, S. V. (1991). ''Water quality implications of Hong Kong's port and airport proposals.'' *Environmental hydraulics*, J. Lee and Y. K. Cheng, eds., Balkema, Rotterdam, The Netherlands, 859–864.